Hindawi
Advances in Mathematical Physics
Volume 2023, Article ID 1410642, 14 pages
https://doi.org/10.1155/2023/1410642

Research Article

Convolution Representation of Traveling Pulses in Reaction-Diffusion Systems

Satoshi Kawaguchi

Department of Complex and Intelligent Systems, School of Systems Information Science, Future University Hakodate, Hakodate 041-8655, Japan

Correspondence should be addressed to Satoshi Kawaguchi; satoshi@fun.ac.jp

Received 5 October 2022; Revised 13 February 2023; Accepted 21 February 2023; Published 30 March 2023

Academic Editor: Luigi C. Berselli

Convolution representation manifests itself as an important tool in the reduction of partial differential equations. In this study, we consider the convolution representation of traveling pulses in reaction-diffusion systems. Under the adiabatic approximation of inhibitor, a two-component reaction-diffusion system is reduced to a one-component reaction-diffusion equation with a convolution term. To find the traveling speed in a reaction-diffusion system with a global coupling term, the stability of the standing pulse and the relation between traveling speed and bifurcation parameter are examined. Additionally, we consider the traveling pulses in the kernel-based Turing model. The stability of the spatially homogeneous state and most unstable wave number are examined. The practical utilities of the convolution representation of reaction-diffusion systems are discussed.

1. Introduction

Many phenomena are described by mathematical and physical models, including traffic flow, stripe of dune, bubble in the granular medium, and plasma flow [1–5]. Among these phenomena, spatio-temporal patterning is one of the attractive topics in the field of nonlinear physics. To describe these patterns by a simple mathematical model, many reaction diffusion (RD) systems have been proposed. In pattern formation in RD systems, the Turing instability is a key concept; the difference in diffusion rates of the activator and inhibitor leads to lateral inhibition. The Turing pattern is caused by lateral inhibition around the excited region: short-range activation and long-range inhibition [6]. Recently, the reduction of a two-component RD system to a one-component RD equation with a convolution term has been considered. Considering that the system converges to a stationary state, the inhibitor is expressed in the form of convolution using the activator. The convolution representation using a weight function, called a kernel, has a nonlocal effect on the activator. A Mexican-hat-type function is often used as a kernel [7–9]. The Mexican-hat-type kernel creates a suppressive region far from the central enhanced region, which imitates the lateral inhibition around the excited region, resulting in pattern formation [10]. In the 1970s, the convolution term was introduced in the time evolution equation of the membrane potential in a neural model [11]. This term caused a nonlocal effect on the membrane potential via the neighbour cells in the network. To choose adequate parameters in a model, the traveling wave was calculated self-consistently. Inspired by this study, traveling waves in a neural network have been considered [12, 13].

Among many Turing patterns in nature, the pigmentation on the skin of zebrafish has been well-reported [14–17]. Fish pigmentation shows many patterns such as spot, stripe, and labyrinth. Critical pigment cells are yellow and black, which form interaction networks, resulting in Turing patterns. This pattern formation has been modeled using a multicomponent RD system. Given the variety of patterns found on the skin of zebrafish, the dependence of pattern formation on the kernel function was studied recently [18]. The multicomponent RD system was reduced to a single-component activator equation with a convolution term, called as kernel-based Turing model (KT model). The Mexican-hat-type kernel composed of two Gaussian functions with reverse sign was employed. Generally, patterns are sensitive to the shape of a kernel; amplitude, width,

distance between centers of a source, and the peak position of the distribution. Therefore, variations in observed patterns in nature are due to variations in the kernel. Additionally, we can predict spatial patterns in two dimensions by using the KT model. That is, we first obtain the most unstable mode (wave number) and the corresponding eigenvalues through linear stability analysis. Considering this information in the kernel, we can predict what pattern will occur when the spatially homogeneous state becomes unstable [19]. From these perspectives, the KT model is expected to be a promising equation for pattern formation. Generally, the KT model is valid when the system converges to a stationary state; transient patterns cannot be described by the KT model.

Aside from the static stationary patterns, many temporally changing patterns exist: stripe patterns in nematic liquid crystal, traveling band in colloidal suspension, traveling waves in shallow-water, and fluidized granular media [20–24]. Although these dynamical patterns were modeled and analyzed by many mathematical methods, not many studies focused on the traveling waves in the RD equation using the kernel function [25–28]. The interaction of traveling pulses and fronts in one dimension described by convolution representation was studied [29]. The interaction between two adjacent waves decayed exponentially with an increase in the distance between them. Although the asymptotic behavior of interacting traveling waves was considered, an explicit traveling wave solution using convolution representation was not given. Stationary traveling waves in one and two dimensions have been observed in experiments [30–32], traveling waves in the RD equation with the convolution representation should be investigated.

In this study, we consider the procedure to transform traveling pulses in RD systems into convolution representation, employing a mathematically tractable RD system. Accordingly, we consider two types of RD systems. The first one is a one-dimensional RD system with a global coupling term. An experimental setup corresponding to the global coupling term has been considered: the current filaments in gas-discharge and *p-n-p-n* diode systems and the chemical reaction on catalytic ribbon surface. In electric circuit systems, although the current filament distributes on the electrode, the total current is feedback-controlled [33, 34]. Similarly, in the chemical reaction on the catalytic ribbon, the spatial average temperature of the surface is kept constant [35]. These feedback controls are modeled by space-averaged terms called global couplings. Although the stability of standing pulse in these systems has been studied, the properties of traveling pulse solutions have not been clarified yet. For the second RD system, we consider a usual two-component RD system with cubic nonlinearity. We derive the KT model from this system and consider localized pulses from the perspective of Turing instability. The remainder of this paper is organized as follows. In Section 2, we introduce an RD system with a global coupling term. We consider the stability of the standing pulse solution and show the relation between the traveling speed and bifurcation parameter. Using these results, we demonstrate the choice of an adequate speed in the kernel representation of traveling pulse. In Section 5, we consider pulse solutions in the KT model. To confirm the validity of numerical simulations, the stability of the spatially homogeneous solution is examined. Finally, the application of our study to experiments and further extensions is discussed in Section 8.

2. RD System with Global Coupling

We first introduce a two-component RD system with a global coupling term in one dimension [36]. Activator u and inhibitor v satisfy the following time evolution equations:

$$\begin{aligned} \tau\varepsilon\frac{\partial u}{\partial t} &= \varepsilon^2\frac{\partial^2 u}{\partial x^2} + f(u,v), \\ \frac{\partial v}{\partial t} &= \frac{\partial^2 v}{\partial x^2} + g(u,v), \end{aligned} \tag{1}$$

where

$$\begin{aligned} f(u,v) &= H(u-a) - u - v, \\ g(u,v) &= u - \mu v, \\ a &= a_0 + \alpha\left(\int (u+v)dx - s_0\right), \end{aligned} \tag{2}$$

where $H(x)$ is the step function satisfying $H(x) = 1$ for $x > 0$ and $H(x) = 0$ for $x < 0$. We choose ε and a_0 such that $0 < \varepsilon \ll 1$ and $0 < a_0 < 1/2$, respectively. τ, μ, and s_0 are positive constants. When the magnitude of global coupling $\alpha = 0$, a is a constant, a_0, and the RD system (1) is a local coupling system, called the McKean model. By contrast, when $\alpha > 0$, the RD system (1) is a global coupling system; when α is large, the second term of a controls such that the width of excited region is s_0 in the limit $\varepsilon \longrightarrow 0$.

Let us briefly summarize the solution of the RD system (1) [37]. First, we consider the case $\alpha = 0$. When τ is large, there is a stationary pulse solution, the standing pulse. Although the pulse has left and right interfaces in the limit $\varepsilon \longrightarrow 0$, these interfaces become a transition layer (inner layer) with a width $O(\varepsilon)$ for finite $\varepsilon(\ll 1)$. On decreasing τ, the standing pulse is destabilized through the oscillatory bifurcation; the interfaces oscillate symmetrically with respect to the center of the pulse (breathing motion). On decreasing τ further, the pulse is secondarily destabilized through the translational bifurcation, resulting in the traveling pulse. The velocity of the traveling pulse increases as decreasing τ. By contrast, when $\alpha > 0$, on decreasing τ, the standing pulse is primarily destabilized through the translational bifurcation; the oscillatory bifurcation is suppressed strongly for large α. The global coupling term in the definition of a suggests the strict restriction of $\int (u+v)dx \sim s_0$ for large α. This condition prohibits the breathing motion of the interface, and the translational bifurcation occurs primarily on decreasing τ.

3. Convolution Representation of the RD System

For smaller τ, the RD system (1) has traveling pulse solutions. We consider the convolution representation of the stationary traveling pulse solution of the RD system (1). In the moving coordinate $z = x - ct$, where $c(\geq 0)$ is a traveling speed, the time evolution equations of $u(z,t)$ and $v(z,t)$ are

$$\begin{aligned} \tau\varepsilon\frac{\partial u}{\partial t} &= \varepsilon^2\frac{\partial^2 u}{\partial z^2} + \tau\varepsilon c\frac{\partial u}{\partial z} + H(u-a) - u - v, \\ \frac{\partial v}{\partial t} &= \frac{\partial^2 v}{\partial z^2} + c\frac{\partial v}{\partial z} + u - \mu v. \end{aligned} \tag{3}$$

In the interval $[-L, L]$, the stationary solution of v in the system (3), subject to periodic boundary conditions, is given in the form of cyclic convolution. The detailed derivation is given in Appendix A, and the final expression is

$$\begin{aligned} v(z) = {} & \frac{1}{2(\lambda_+ - \lambda_-)}\frac{1}{\sinh(\lambda_+ L)\sinh(\lambda_- L)} \\ & \times \left[\int_{-L}^{z}\left\{e^{\lambda_+(z-L-y)}\sinh(\lambda_- L) - e^{\lambda_-(z-L-y)}\sinh(\lambda_+ L)\right\}u(y)dy\right. \\ & \left. + \int_{z}^{L}\left\{e^{\lambda_+(z+L-y)}\sinh(\lambda_- L) - e^{\lambda_-(z+L-y)}\sinh(\lambda_+ L)\right\}u(y)dy\right], \end{aligned} \tag{4}$$

where $\lambda_\pm = (-c \pm \sqrt{c^2 + 4\mu})/2$. Using Equation (4), the time evolution of $u(z,t)$ is

$$\begin{aligned} \tau\varepsilon\frac{\partial u}{\partial t} &= \varepsilon^2\frac{\partial^2 u}{\partial z^2} + \tau\varepsilon c\frac{\partial u}{\partial z} + H(u-a) - u - v \\ &= \varepsilon^2\frac{\partial^2 u}{\partial z^2} + \tau\varepsilon c\frac{\partial u}{\partial z} + H(u-a) - u - J * u(z), \end{aligned} \tag{5}$$

where J corresponds to a kernel and the cyclic convolution $J * u(z)$ is defined as

$$J * u(z) = \int_{-L}^{L} J(z-y)u(y)dy, \tag{6}$$

with

$$\begin{aligned} J(z) = {} & \frac{1}{2(\lambda_+ - \lambda_-)}\frac{1}{\sinh(\lambda_+ L)\sinh(\lambda_- L)} \\ & \cdot \left\{e^{\lambda_+(z - \operatorname{sgn}(z)L)}\sinh(\lambda_- L) - e^{\lambda_-(z-\operatorname{sgn}(z)L)}\sinh(\lambda_+ L)\right\}, \end{aligned} \tag{7}$$

where sgn is a sign function, satisfying $\operatorname{sgn}(x) = 1$ for $x > 0$ and -1 for $x < 0$. For sufficiently large L with $c = 0$, kernel Equation (7) is approximately $J \sim \exp(-\sqrt{\mu}|z|)/2\sqrt{\mu}$, the kernel for diffusion. When $c = 0$ with $\mu = 1$, we note that Equation (7) recovers the results in ref. [38]. Equation (5) yields a time evolution of $u(z,t)$ for a given initial condition $u(z, t = 0)$ until $u(z,t)$ converges to a stationary solution; it is valid for given c, τ, and α, for which the RD system (3) has a stationary traveling pulse. Unlike the Korteweg-de Vries (KdV) equation [39], traveling speed c is not arbitrary. To find the adequate value of c for given τ and α, we perform stability analysis of the standing pulse in the RD system (1).

4. Stability Analysis Using a Singular Perturbation Method

For the RD system (1), the stability of the standing pulse is examined using the singular perturbation method [37, 40]. The exponential growth of perturbation to the standing pulse solution $(\eta_0, \bar{v}(x))$ is determined by the roots of $F_\pm(z) = 0$. Here, $l = 2\eta_0$ is the standing pulse width, and $\bar{v}(x)$ is a stationary solution, symmetric with respect to $x = 0$, of the RD system (1) in the limit $\varepsilon \longrightarrow 0$. The brief derivation of the stability formula $F_\pm(z)$ is given in Appendix B, and the final expression is

$$\begin{aligned} F_\pm(z) = {} & -z + \frac{4}{\tau}\left(\frac{1}{2\sqrt{\mu+1}}\left(1 - e^{-2\sqrt{\mu+1}\eta_0}\right)\right. \\ & \left. - \frac{1}{2\sqrt{z+\mu+1}}\left(1 \pm e^{-2\sqrt{z+\mu+1}\eta_0}\right) + (1 \pm 1)\alpha\right). \end{aligned} \tag{8}$$

In the derivation of Equation (8), we assumed that perturbations were supplied to the stationary position, and the left and right interface positions were shifted as $l_1(t) = -\eta_0 + \xi_1(t)$ and $l_2(t) = \eta_0 + \xi_2(t)$, respectively. We consider two modes of perturbation: the symmetric perturbation with respect to the center of the pulse $-\xi_1 = \xi_2 = \xi$ and antisymmetric one $\xi_1 = \xi_2 = \xi$. F_+ and F_- correspond to the symmetric and antisymmetric cases, respectively. We observe that $F_-(0) = 0$, which corresponds to the translational invariance. When $F_-(z)$ is degenerated at $z = 0$, that is,

$$F_-(0) = \frac{dF_-(0)}{dz} = 0, \tag{9}$$

the standing pulse is destabilized through the translational bifurcation; condition (9) gives τ_t as

$$\tau_t = (\mu+1)^{-3/2}\left[\left(1 - e^{-2\sqrt{\mu+1}\eta_0}\right) - 2\eta_0\sqrt{\mu+1}e^{-2\sqrt{\mu+1}\eta_0}\right]. \tag{10}$$

Meanwhile, when $F_+(z) = 0$ has a pair of the imaginary solutions $\pm ik$ with real number k, the standing pulse is destabilized through the oscillatory bifurcation; interfaces oscillate symmetrically with respect to the center of the pulse. This condition gives τ_o, which is given by the solution

$$F_+(ik) = 0. \tag{11}$$

Using these formula, we consider the dependence of bifurcation of standing pulse on τ and α in Section 7.

5. Traveling Pulse Solution of the KT Model

In the above discussion, we considered the convolution representation of traveling pulse in an RD system where the inhibitor was expressed by using kernel integral in the stationary state. By contrast, there is another type of RD equation with convolution representation: the KT model. The Mexican-hat-type kernel is employed in this model.

Let us consider the following RD system with a cubic nonlinear function in the activator:

$$\begin{aligned}\varepsilon\frac{\partial u}{\partial t} &= \varepsilon^2\frac{\partial^2 u}{\partial x^2} + f(u,v),\\ \frac{\partial v}{\partial t} &= \frac{\partial^2 v}{\partial x^2} + g(u,v),\end{aligned} \tag{12}$$

where

$$\begin{aligned}f(u,v) &= u(1-u)(u-a_0) - v,\\ g(u,v) &= u - \mu v,\end{aligned} \tag{13}$$

where a_0 is a constant in the range $0 < a_0 < 1$. We consider the stationary pulse solutions in the interval $[-L, L]$ under periodic boundary conditions. We use the Mexican-hat-type kernel, which causes the activation in the short range while suppressing it in the long range.

To consider the traveling pulse, we introduce the moving coordinate $z = x - ct$, where c is a traveling speed. Following a similar procedure as in Section 3, the RD equation with a convolution term, the KT model, is proposed

$$\varepsilon\frac{\partial u}{\partial t} = \varepsilon^2\frac{\partial^2 u}{\partial z^2} + \varepsilon c\frac{\partial u}{\partial z} + u(1-u)(u-a_0) + J * u(z), \tag{14}$$

where

$$J * u(z) = \int_{-L}^{L} J(z-y)u(y)dy, \tag{15}$$

with kernel J

$$\begin{aligned}J(z) = {} & \frac{1}{2d_1(\lambda_+ - \lambda_-)}\frac{1}{\sinh(\lambda_+ L)\sinh(\lambda_- L)}\\ & \times\left\{e^{\lambda_+(z-\operatorname{sgn}(z)L)}\sinh(\lambda_- L) - e^{\lambda_-(z-\operatorname{sgn}(z)L)}\sinh(\lambda_+ L)\right\}\\ & - \frac{1}{2d_2\left(\widehat{\lambda}_+ - \widehat{\lambda}_-\right)}\frac{1}{\sinh\left(\widehat{\lambda}_+ L\right)\sinh\left(\widehat{\lambda}_- L\right)}\\ & \times\left\{e^{\widehat{\lambda}_+(z-\operatorname{sgn}(z)L)}\sinh\left(\widehat{\lambda}_- L\right) - e^{\widehat{\lambda}_-(z-\operatorname{sgn}(z)L)}\sinh\left(\widehat{\lambda}_+ L\right)\right\},\end{aligned} \tag{16}$$

where $\lambda_\pm = [-(c/d_1) \pm \sqrt{(c/d_1)^2 + 4(\mu/d_1)}]/2$ and $\widehat{\lambda}_\pm = [-(c/d_2) \pm \sqrt{(c/d_2)^2 + 4(\mu/d_2)}]/2$. When $c = 0$, Equation (16) recovers the kernel of a standing pulse in ref. [38]. To make the Mexican-hat-type kernel, we assume that $d_1 = 1$ and d_2 is under condition $d_1 < d_2$. The KT model (14) is the time evolution equation of $u(z,t)$ with an initial condition $u(z, t = 0)$, which is valid until $u(z,t)$ converges to a stationary solution. In the KT model, parameters d_1, d_2, and c are not restricted, except for condition $d_1 < d_2$.

In Section 3, Equation (6) represents stationary solution of $v(z)$, and Equation (7) corresponds to its kernel, which is composed of a single term. By contrast, in the KT model, the kernel Equation (16) is composed of two similar terms with the reverse sign. Because $d_2 > d_1$, the second term of Equation (16) operates suppressively on u far from the center of the pulse. For a larger d_2, a suppressive region of the kernel is wider.

6. Linear Stability of the Homogeneous Solution of the KT Model

In this section, we consider the Turing instability in a two-component RD system (12). There is a spatially homogeneous solution of the RD system (12); $u = v = 0$. The KT model corresponding to the RD system (12) is proposed as

$$\varepsilon\frac{\partial u}{\partial t} = \varepsilon^2\frac{\partial^2 u}{\partial x^2} + h(u), \tag{17}$$

where

$$h(u) = u(1-u)(u-a_0) + v(u) = u(1-u)(u-a_0) + J * u(x), \tag{18}$$

and J is given by Equation (16) with $c = 0$.

We consider the pulse solution of the KT model (17) in the interval $[-L, L]$ under periodic boundary conditions. To clarify the mechanism of the pulse solution occurrence in the KT model (17), we consider the linear stability of the spatially homogeneous solution. The growth rate of instability is obtained through linear stability analysis. A brief derivation is given in Appendix D, and the eigenvalue is

$$\lambda = \frac{1}{\varepsilon}\left[-\left(\frac{\varepsilon k\pi}{L}\right)^2 + 2LJ_k - a_0\right], \tag{19}$$

where J_k is

$$\begin{aligned}J_k = \frac{1}{2L}\Bigg[& -\frac{1}{d_1(\lambda_+ - i(k\pi/L))(\lambda_- - i(k\pi/L))}\\ & + \frac{1}{d_2\left(\widehat{\lambda}_+ - i(k\pi/L)\right)\left(\widehat{\lambda}_- - i(k\pi/L)\right)}\Bigg],\end{aligned} \tag{20}$$

and k represents the wave number that takes the values of $0, \pm 1, \pm 2, \cdots$. $\lambda_\pm$ and $\widehat{\lambda}_\pm$ are given in Section 5. Although the above eigenvalue is derived for the stationary state with $c = 0$, the formulation is valid in the moving coordinate system with finite c. The linear stability analysis of the spatially

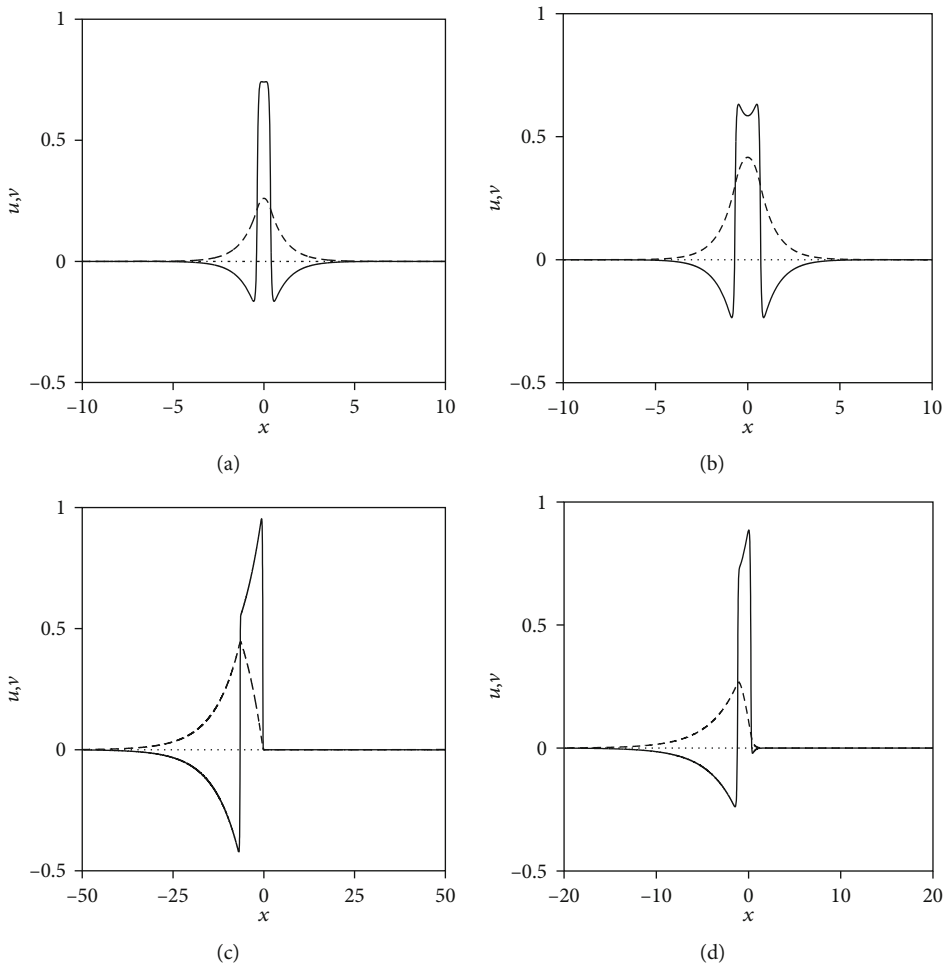

FIGURE 1: Profiles of the pulse in the RD system (1) under periodic boundary conditions. Solid and dashed curves represent u and v, respectively. $L = 50$. (a) Standing pulse. $\tau = 0.4$ and $\alpha = 0$. (b) Standing pulse. $\tau = 0.4$, $\alpha = 3$, and $s_0 = 1.4$. (c) Traveling pulse. $\tau = 0.1$ and $\alpha = 0$. (d) Traveling pulse. $\tau = 0.1$, $\alpha = 3$, and $s_0 = 1.4$.

homogeneous solution in the two-component RD system was considered in refs. [6, 7]. The eigenvalue was given by a quadratic function in terms of k^2 resulting from the diffusion terms of the activator and inhibitor in the system. By contrast, in the stability analysis of the KT model, the diffusion of the inhibitor is considered in the kernel function. This results in a different expression of an eigenvalue. Using this formula, we consider the validity of the pulse solutions in the KT model in Section 7.

7. Numerical Results

In this section, we consider the numerical results. In the calculation of the RD system (1), the time evolution of u using kernel representation Equations (5) and (14), we fix $\varepsilon = 5 \times 10^{-2}$, $a_0 = 0.275$, $\mu = 0.3$, and $d_1 = 1$ and choose differences $\Delta x = 1 \times 10^{-2}$ and $\Delta t = 5 \times 10^{-5}$. The calculation of spatial direction is performed using an implicit method, Crank-Nicolson method, under periodic boundary conditions. Here, x is in the range of $x \in [-L, L]$.

We first show the profiles of u and v of the stationary pulses in the RD system (1) in Figure 1. The standing pulse is symmetric with respect to $x = 0$ and remains in the same position. Although the standing pulse is stable for large τ, it is destabilized through the translational bifurcation on decreasing τ. The traveling pulse moves to the right direction with a constant speed. The traveling speed and pulse width are determined self-consistently in the RD system (1).

To consider the stability of the stationary standing pulse, we show the dependence of the pulse width on α [37]. We consider the symmetric standing pulse with respect to $x = 0$, the position of interface is $x = \pm\eta_0$, and the pulse width $l = 2\eta_0$. There are two cases depending on s_0, as shown in Figure 2. When $\alpha = 0$, $\eta_0 = \bar{\eta}_0$, on increasing α, η_0 changes and converges to η_0^*. The stability of the standing pulse is calculated using $F_\pm$. The result is shown in Figure 3. When $\alpha = 0$, the standing pulse is first destabilized through the oscillatory bifurcation on decreasing τ. By contrast, for large finite values of α, the oscillatory bifurcation is suppressed, and the standing pulse is first destabilized through the translational bifurcation on decreasing τ. The suppression of the oscillatory bifurcation by global coupling results from the conservation of the pulse width. Under strong global coupling, although the deviation of the pulse width is strictly

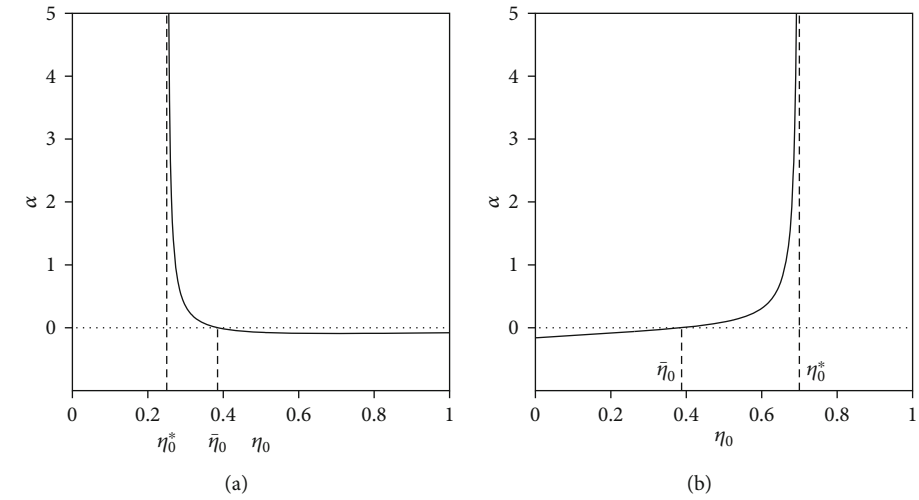

FIGURE 2: η_0-α relation of a standing pulse of the RD system (1). (a) $s_0 = 0.5$. (b) $s_0 = 1.4$.

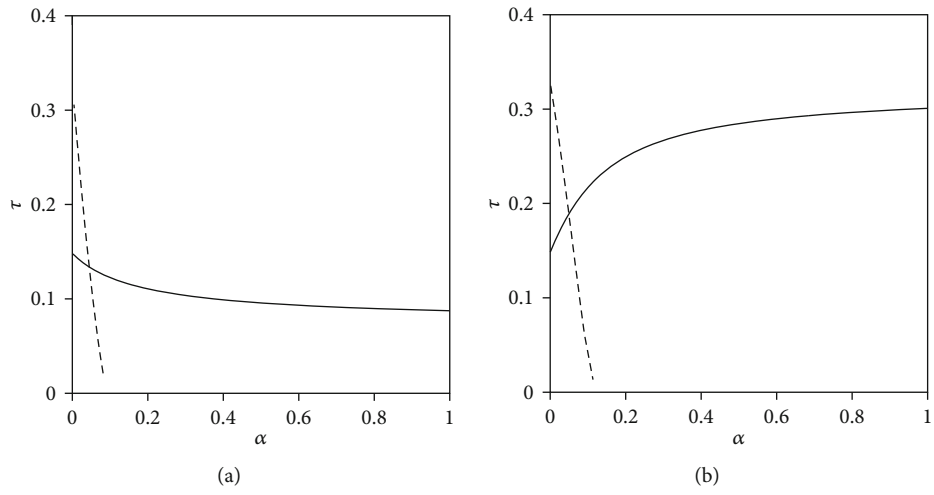

FIGURE 3: Bifurcation diagrams of a standing pulse. The data are obtained by the singular perturbation method in the limit $\varepsilon \longrightarrow 0$. Solid and dashed curves represent τ_t and τ_o, respectively. (a) $s_0 = 0.5$. (b) $s_0 = 1.4$.

prohibited, the translational motion with the same width is allowed. We briefly summarize the stability of the standing pulse solution of the RD system (1). When $\alpha = 0$, the RD system (1) is a local coupling system, and standing pulse solutions exist for large τ. On decreasing τ, the standing pulse solutions are destabilized through the oscillatory bifurcation, and the interfaces oscillate (breathing motion). On decreasing τ further, the standing pulses with breathing motion bifurcate secondarily to traveling pulse solutions. By contrast, when $\alpha > 0$, the RD system (1) is a global coupling system. Although standing pulse solutions exist for large τ, the standing pulse is destabilized through a translational bifurcation on decreasing τ because the oscillatory bifurcation is suppressed. Thus, the traveling pulses primarily occur on decreasing τ.

Although the traveling speed of the soliton solution of the KdV equation is an arbitrary parameter, that of the RD system is determined self-consistently. To obtain a stationary traveling pulse solution by using Equation (5), it is necessary to choose an adequate value of c for given τ and α. Accordingly, we first consider the dependences of velocity c on τ and l, where l is defined as the interval of two interfaces in the limit $\varepsilon \longrightarrow 0$. The relation between c, τ, and l is calculated self-consistently by using $C(v_i, a)$ (given by Equation (B.1)), where v_i represents $v(z)$ evaluated at interface positions $z = z_{\pm}$. The brief derivation of $v(z)$ is given in Appendix C. The dependence of c on τ is shown in Figure 4(a). For $\alpha = 0$, the traveling pulse appears subcritically at $\tau_c \sim 0.2072$; the traveling pulse appears suddenly with a finite value of c, which increases with decreasing τ [41–44]. By contrast, for $\alpha = 3$ with $s_0 = 1.4$, the traveling pulse appears supercritically at $\tau_c \sim 0.312$ with $c = 0$. The dependence of c on l is shown in Figure 4(b). For $\alpha = 0$, c increases with increasing l. By contrast, for $\alpha = 3$, c increases in small range of l, which is almost constant. This property results from the strong global coupling in the RD system (1); the oscillatory instability is suppressed strongly [36, 37]. By the definition of a, Equation (2), the

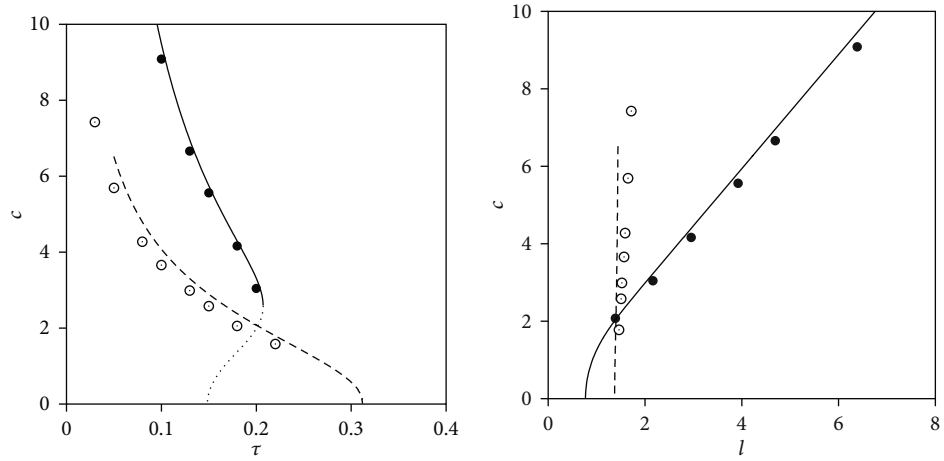

FIGURE 4: Dependence of traveling speed c on τ and pulse width l. Symbols • and ◦ represent simulation results of the RD system (1) in the case of $\alpha = 0$ and 3, respectively. (a) Dependence of speed on τ. Solid curve represents the case of $\alpha = 0$ and which connects with the unstable branch (dotted curve) at $\tau \sim 0.2072$ ($\equiv \tau_c$). Dashed curve represents the case of $\alpha = 3$ with $s_0 = 1.4$. $\tau_c \sim 0.312$. (b) Dependence of speed on l. Solid and dashed curves represent the cases of $\alpha = 0$ and $\alpha = 3$ with $s_0 = 1.4$, respectively.

pulse width l is s_0 for large α in the limit $\varepsilon \longrightarrow 0$. From these results, the value of c for chosen τ and α is restricted such that the standing pulse is destabilized through the translational bifuraction; here, τ is less than τ_t. Additionally, τ should be less than τ_c to find the value of c on τ-c relation, as shown in Figure 4(a). For $\alpha = 0$, the value of c is chosen on the upper branch with solid curve in Figure 4(a); the upper (lower) branch is stable (unstable) [41, 44]. In the case of $\alpha > 0$, the lower branch disappears, and the value of c is chosen on the dashed curve in Figure 4(a). The dependences of c on τ and l are confirmed by the simulation of the RD system (1). The data points are in good agreement with theoretical curves, except for a small value of c. This discrepancy results from the fact that ε is chosen small but a finite value in the RD system (1).

Thus, we have considered the stability of the standing pulse and its dependence on α, τ, and s_0 in the two-component RD system (1). Consequently, the standing pulse is destabilized by decreasing τ. Based on this knowledge, we consider the traveling pulse in a one-component RD equation with a convolution term (5). The kernel J given by Equation (7) is shown in Figure 5. When $c = 0$, the kernel is symmetric with respect to $z = 0$ and is positive for all z. We note that the kernel is not a Mexican-hat type. Although there is no suppressive region in the kernel, the convolution term $J * u$ operates suppressively on u in Equation (5) owing to its sign: minus sign as $-J * u$. On increasing c, the kernel becomes asymmetric with respect to $z = 0$ and remains a positive value (see dashed curve in Figure 5). The convolution term $J * u$ maintains the traveling pulse solution for $c > 0$. As examples of the pulse, choosing the adequate values of c and τ, the profiles of u and v of the stationary pulse in Equation (5) are shown in Figure 6. Initial condition $u(z, t = 0)$ was given by a small positive excitation at $z = 0$. Comparing the profiles of u and v in Figure 6 with that in Figure 1, we note that these agree well with each other. Thus, both the standing and traveling pulses in the

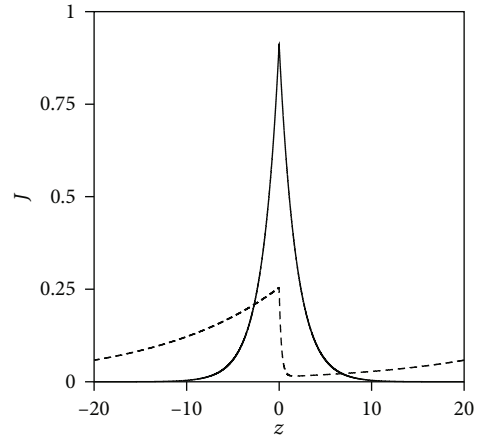

FIGURE 5: Profiles of the kernel given by Equation (7) under periodic boundary conditions. $L = 20$. Solid and dashed curves represent cases of $c = 0$ and 4, respectively.

RD system (1) are recovered by using Equation (5) with an adequate value of c determined by Figure 4(a). We note that the pulse solutions calculated by using Equation (5) are valid in the stationary state and the profiles in the transient state do not agree with those in the RD system (1).

Let us consider the pulse solutions of the KT model (14). The profiles of the kernel Equation (16) are shown in Figure 7(a). The kernel of the KT model is composed of two similar terms with reverse sign, and its profile is a Mexican-hat type. Although the kernel is positive around the center, it is negative far from the center. Using the KT model (14), the profiles of u in the stationary state are calculated, where the initial condition $u(z, t = 0)$ was given by a random number with an amplitude of $|u(z, t = 0)| \leq 0.1$. The stationary profiles of u are shown in Figure 7(b). When $c = 0$, the profile represents the standing pulse (solid curve). When c is chosen positive, the profile represents the

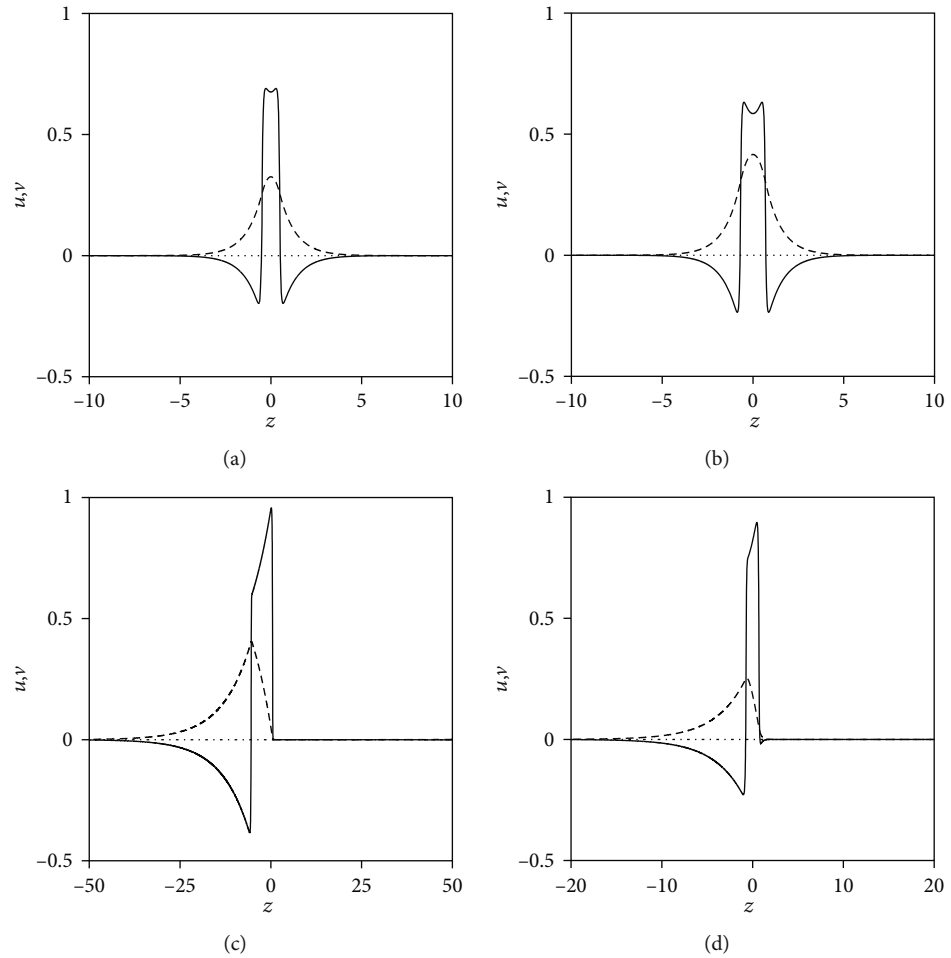

Figure 6: Profiles of the stationary pulse in a one-component RD equation with a convolution term (5) under periodic boundary conditions. Solid and dashed curves represent u and v, respectively. $L = 50$. (a) Standing pulse. $\tau = 0.4$, $\alpha = 0$, and $c = 0$. (b) Standing pulse. $\tau = 0.4$, $\alpha = 3$, $s_0 = 1.4$, and $c = 0$. (c) Traveling pulse. $\tau = 0.1$, $\alpha = 0$, and $c = 10$. (d) Traveling pulse. $\tau = 0.1$, $\alpha = 3$, $s_0 = 1.4$, and $c = 4$.

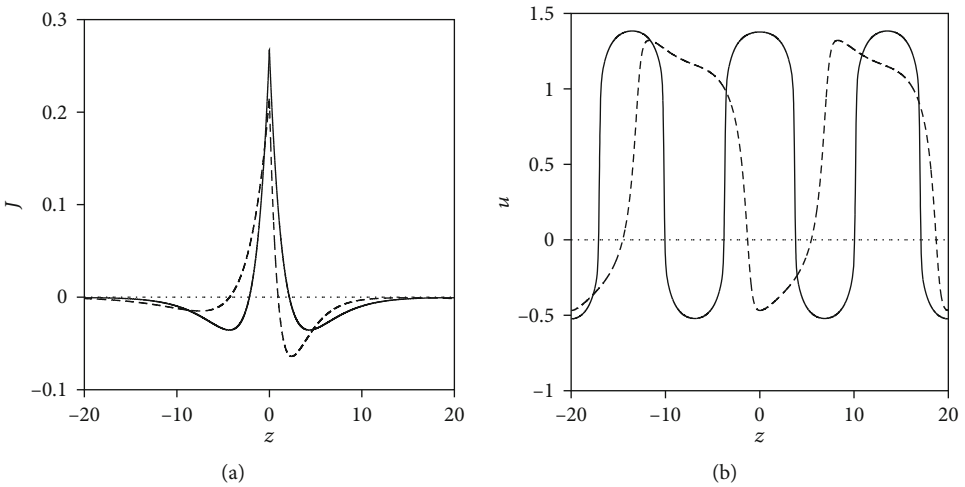

Figure 7: Profiles of the kernel given by Equation (16) and the stationary solution of the KT model (14) under periodic boundary conditions. $d_2 = 2$ and $L = 20$. Solid and dashed curves represent cases of $c = 0$ and 0.5, respectively. (a) Profiles of the kernel. (b) Profiles of the stationary solution.

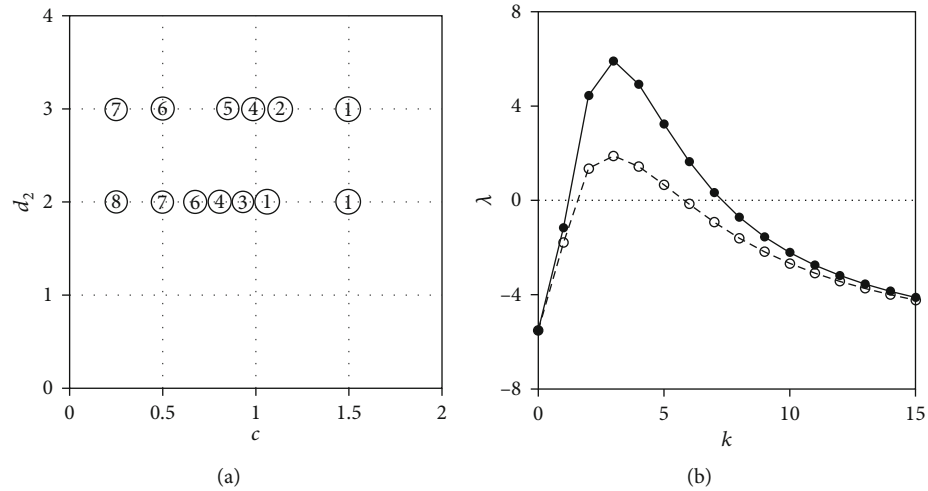

FIGURE 8: Number of pulses in the KT model (14) in a large system and dependence of eigenvalues on the wave number given by Equation (19). (a) Dependence of number of pulses in (c, d_2) space. Numbers in the figure represent the number of the pulses in the system size $L = 60$. (b) Dependence of eigenvalues λ on the wave number k given by Equation (19). Symbols • and ◦ represent eigenvalues in the case of $c = 0$ and 0.5, respectively. $d_2 = 2$ and $L = 20$.

traveling pulse with the right direction in the moving coordinate $z = x - ct$ (dashed curve). For sufficiently large c, there remains only one traveling pulse in the system. The pulse number depends on c and d_2, as shown in Figure 8(a). As increasing c and d_2, asymmetry of the pulse is remarkable, and the interval of pulses is larger due to the strong lateral inhibition; the number of pulses in the system is reduced. To confirm the validity of the occurrence of the pulse solution in the KT model, the stability of a spatially homogeneous solution $(u = 0)$ is considered by using Equation (19). The dependence of eigenvalue λ on wave number k is shown in Figure 8(b). When λ is positive, the corresponding wave number destabilizes the homogeneous solution. The figure suggests that the homogeneous solution is unstable for $k = 2, 3, \cdots, 6$. The most unstable mode, by which the maximum eigenvalue is attained, is $k = 3$ for both $c = 0$ and 0.5. In our simulation of the KT model (14), we obtain three (two) standing (traveling) pulses for $c = 0(0.5)$, as shown in Figure 7(b). Thus, the number of pulses obtained by the simulation is reasonable, and the occurrence of pulses results from the Turing instability.

8. Conclusions

In this study, we considered the convolution representation of traveling pulses in a two-component RD system and the KT model. For analytical tractability, a McKean-type nonlinearity was adopted in a two-component RD system (1) with Equation (2). Under the assumption that the relaxation of an inhibitor was fast, a two-component RD system was reduced to a one-component RD equation with a convolution term given by Equation (5). To obtain the stationary standing pulse or traveling pulse by using Equation (5), it was necessary to proceed with numerical calculations until an activator u converged to a stationary state. When the RD system (1) did not converge to a stationary state, our formulation was not valid. Additionally, the transient state calculated by using Equation (5) did not agree with that calculated by the RD system (1). In the one-component RD equation with a convolution term given by Equation (5), the traveling speed c was unknown a priori. To find an adequate value of c, the stability analysis of the standing pulse of the RD system (1) and τ-c relation was necessary. The fluctuation of parameter τ around the bifurcation point in the case of the strong global coupling was much smaller than that in the case of local coupling. This is because that the oscillatory instability was strongly prohibited under a strong global coupling and the standing pulse was primarily destabilized through the translational bifurcation. Using an adequate value of c for a chosen τ, we could obtain the stationary traveling pulse solution.

By contrast, in the previous studies of the KT model [18, 38], it was shown that a stationary standing pulse occurred using a symmetric Mexican-hat-type kernel. As the extension to the traveling pulse, we have shown that the traveling pulse was described by the asymmetric Mexican-hat-type kernel. The spatially homogeneous solution was destabilized through the Turing instability, and the stationary standing or traveling pulses occurred. In a multicomponent RD system, the Turing instability is caused by different magnitudes of the diffusion of activators and inhibitors. In the KT model, the kernel was composed of different magnitudes of a Gaussian-type function with a reverse sign, which formed the Mexican-hat-type kernel. The difference between d_1 and d_2 created a lateral inhibition, resulting in the localized standing or traveling pulses. The number of pulses in the system corresponded to the most unstable mode of the wave number. Because there is no restriction on parameters d_1, d_2, and c in the KT model, it is necessary to choose them by considering other types of information, for example, matching patterns in the model with experimental observations. Another method to determine the parameters

is to match the most unstable wave number obtained through the linear stability analysis with observation. The most unstable wave number is determined self-consistently by d_1, d_2, c, and L under the periodic boundary conditions.

We discuss the practical utilities of the convolution representation of RD systems. First, we discuss the global coupling system in the experiments. The current filament in the gas-discharge system [45, 46] corresponds directly to the theoretical model [36]. The total current in these gas-discharge systems is calculated by the integral of the current density over the electrode. The external resistor R_0 in the circuit corresponds to the magnitude of global coupling α. On decreasing R_0, the total current is increased, and the sequence of transition of current filament occurs; on decreasing R_0, the spatially homogeneous filament is destabilized to a localized filament, an oscillatory filament (a rocking current filament; antisymmetric oscillation keeping a total current constant), and finally, a traveling filament. The difference between the experimental setup and theoretical model is that the integrand is the sum of the activator and inhibitor in the theoretical model [36]. Although this assumption is unpractical, the physics remains the same. When the traveling pulse is described by using a one-component RD equation with a convolution term, an adequate traveling speed c is obtained following our procedures.

Second, we consider the m-component RD system. There are many experimental setups that show traveling waves in one and two dimensions, such as nematic liquid crystal, camphor boat, and action potential in nerves [47–49]. Reducing the multicomponent RD system to a single-component RD equation with a convolution term (the KT model), it is necessary to determine d_i ($i = 1, 2, \cdots, m$), c, and L in the kernel. The stability condition of the spatially homogeneous solution is obtained by following similar procedures with this study. The most unstable wave number coincides with the number of waves in the system. Thus, d_i, c, and L can be chosen such that the numerical results by the KT model match with the observed pattern. The multicomponent RD system or complicated cascade reactions can be reduced to an equivalent KT model, and the parameters in the kernel are determined by the above procedures.

Appendix

A. Derivation of the Kernel Function of a Traveling Pulse

In this appendix, we briefly derive the kernel of a traveling pulse in an RD system (1). The equations of an RD system are

$$\begin{aligned} \tau\varepsilon\frac{\partial u}{\partial t} &= \varepsilon^2\frac{\partial^2 u}{\partial x^2} + f(u,v), \\ \frac{\partial v}{\partial t} &= \frac{\partial^2 v}{\partial x^2} + g(u,v), \end{aligned} \tag{A.1}$$

where $f(u,v) = H(u-a) - u - v$ and $g(u,v) = u - \mu v$. In the moving coordinate $z = x - ct$, Equation (A.1) is

$$\begin{aligned} \tau\varepsilon\frac{\partial u}{\partial t} &= \varepsilon^2\frac{\partial^2 u}{\partial z^2} + \tau\varepsilon c\frac{\partial u}{\partial z} + f(u,v), \\ \frac{\partial v}{\partial t} &= \frac{\partial^2 v}{\partial z^2} + c\frac{\partial v}{\partial z} + g(u,v). \end{aligned} \tag{A.2}$$

In the stationary state, the left-hand side of Equation (A.2) is zero. We derive the stationary solution $v(z)$ in the interval $[-L, L]$ under the periodic boundary conditions. The stationary solution $v(z)$ is obtained by applying the variation of parameters as

$$\begin{aligned} v(z) = {} & C_1 e^{\lambda_+ z} + C_2 e^{\lambda_- z} + \frac{1}{2(\lambda_+ - \lambda_-)} \\ & \cdot \left[\int_{-L}^{z}\left(e^{\lambda_-(z-y)} - e^{\lambda_+(z-y)}\right)u(y)dy \right. \\ & \left. + \int_{z}^{L}\left(e^{\lambda_+(z-y)} - e^{\lambda_-(z-y)}\right)u(y)dy\right], \end{aligned} \tag{A.3}$$

where $\lambda_\pm = (-c \pm \sqrt{c^2 + 4\mu})/2$ and $C_{1,2}$ are coefficients. Imposing the periodic boundary conditions, $v(-L) = v(L)$ and $dv(-L)/dz = dv(L)/dz$, on Equation (A.3), we can determine $C_{1(2)}$ as

$$\begin{aligned} C_1 &= \frac{1}{4(\lambda_+ - \lambda_-)}\frac{1}{\sinh(\lambda_+ L)}\int_{-L}^{L}\left(e^{\lambda_+(L-y)} + e^{-\lambda_+(L+y)}\right)u(y)dy, \\ C_2 &= \frac{-1}{4(\lambda_+ - \lambda_-)}\frac{1}{\sinh(\lambda_- L)}\int_{-L}^{L}\left(e^{\lambda_-(L-y)} + e^{-\lambda_-(L+y)}\right)u(y)dy. \end{aligned} \tag{A.4}$$

Substituting Equation (A.4) into Equation (A.3), we finally obtain $v(z)$ as

$$\begin{aligned} v(z) = {} & \frac{1}{2(\lambda_+ - \lambda_-)}\frac{1}{\sinh(\lambda_+ L)\sinh(\lambda_- L)} \\ & \times \left[\int_{-L}^{z}\left\{e^{\lambda_+(z-L-y)}\sinh(\lambda_- L) - e^{\lambda_-(z-L-y)}\sinh(\lambda_+ L)\right\}u(y)dy \right. \\ & \left. + \int_{z}^{L}\left\{e^{\lambda_+(z+L-y)}\sinh(\lambda_- L) - e^{\lambda_-(z+L-y)}\sinh(\lambda_+ L)\right\}u(y)dy\right]. \end{aligned} \tag{A.5}$$

We note that Equation (A.5) is in the form of cyclic convolution. Defining the convolution $J * h(z) = \int_{-L}^{L} J(z-y)h(y)dy$ with kernel J, $v(z)$ is expressed as

$$\begin{aligned} v(z) &= \frac{1}{2(\lambda_+ - \lambda_-)} \frac{1}{\sinh(\lambda_+ L)\sinh(\lambda_- L)} \\ &\quad \times \int_{-L}^{L} \Big\{ e^{\lambda_+ (z - \operatorname{sgn}(z-y) L - y)} \sinh(\lambda_- L) \\ &\quad - e^{\lambda_- (z - \operatorname{sgn}(z-y) L - y)} \sinh(\lambda_+ L) \Big\} u(y) dy \\ &\equiv \int_{-L}^{L} J(z-y) u(y) dy, \end{aligned} \tag{A.6}$$

where $J(z)$ is given by Equation (7) and sgn is a sign function, satisfying $\operatorname{sgn}(x) = 1$ for $x > 0$ and -1 for $x < 0$. In the derivation of Equation (A.3), we assumed that $v(z,t)$ is in the stationary state. This assumption corresponds to the adiabatic approximation; v is a fast variable compared to u and is regarded as a stationary state.

B. Stability Formula by a Singular Perturbation Method

In this appendix, following the singular perturbation method [40], we derive briefly the stability formula $F_\pm$ given in Section 4. In a stationary state, we consider symmetric solution with respect to $x = 0$. Here, $(\bar{u}(x), \bar{v}(x))$ denotes the stationary standing pulse solution of the RD system (1) in the limit $\varepsilon \longrightarrow 0$, the interfaces are located at $x = \pm\eta_0$, and the pulse width is $2\eta_0$. Perturbations are supplied to the standing pulse solution; we assume that the left and right interface positions are shifted as $l_1(t) = -\eta_0 + \xi_1(t)$ and $l_2(t) = \eta_0 + \xi_2(t)$, respectively.

The velocity of the pulse is given (for derivation, see ref. [42]) by

$$C(v,a) = \frac{1}{\tau} \frac{2(1/2 - a - v)}{[(a+v)(1-a-v)]^{1/2}}, \tag{B.1}$$

where $a = a_0 + \alpha(2\eta_0 + \xi_2 - \xi_1 - s_0)$. Using Equation (B.1), the equations of motion on the left front at $x = l_1$ and the right front at $x = l_2$ are given by

$$\begin{aligned} \frac{dl_1}{dt} &= -C(v(l_1), a), \\ \frac{dl_2}{dt} &= C(v(l_2), a), \end{aligned} \tag{B.2}$$

respectively, and $v(l_{1(2)})$ corresponds to v evaluated at the interface position $x = l_{1(2)}$. We expand $v(x)$ around the interface position, as $v = v_0 + v_1(t) + v_2(t)$, where v_0 corresponds to v at $x = \pm\eta_0$ in the stationary state. The velocity $C(v,a)$ is expanded around v_0 with $\hat{a}_0 (= a_0 + \alpha(2\eta_0 - s_0))$ as

$$C(v,a) = C(v_0, \hat{a}_0) + \left.\frac{\partial C}{\partial v}\right|_0 (v_1 + v_2) + \left.\frac{\partial C}{\partial a}\right|_0 \hat{a}_1, \tag{B.3}$$

where $C(v_0, \hat{a}_0) = 0$ and $\hat{a}_1(t) = \alpha(\xi_2 - \xi_1)$ and $A|_0$ represents A evaluated using $v = v_0$ with $a = \hat{a}_0$. After several calculations, we obtain

$$\begin{aligned} v_0(\pm\eta_0) &= \frac{1}{\mu+1} e^{-\sqrt{\mu+1}\eta_0} \sinh\sqrt{\mu+1}\eta_0, \\ v_1(-\eta_0 + \xi_1) &= \frac{1}{2\sqrt{\mu+1}} \left(1 - e^{-2\sqrt{\mu+1}\eta_0}\right) \xi_1, \\ v_1(\eta_0 + \xi_2) &= -\frac{1}{2\sqrt{\mu+1}} \left(1 - e^{-2\sqrt{\mu+1}\eta_0}\right) \xi_2, \\ v_2(-\eta_0 + \xi_1) &= \frac{1}{2\pi} \int dq \int_0^t D_q^{(1)}\left(t - t'\right) e^{-\left(q^2+\mu+1\right)t' - iq\eta_0} dt', \\ v_2(\eta_0 + \xi_2) &= \frac{1}{2\pi} \int dq \int_0^t D_q^{(1)}\left(t - t'\right) e^{-\left(q^2+\mu+1\right)t' + iq\eta_0} dt', \end{aligned} \tag{B.4}$$

where $D_q^{(1)}$ is given by

$$D_q^{(1)}\left(t - t'\right) = -\left(e^{iq\eta_0}\xi_1\left(t - t'\right) - e^{-iq\eta_0}\xi_2\left(t - t'\right)\right). \tag{B.5}$$

To express Equation (B.2) in a linear form of ξ_1 and ξ_2, we define the Laplace transformation of $\xi(t)$ as

$$\widehat{\xi}(z) = \int_0^\infty \xi(t) e^{-zt} dt. \tag{B.6}$$

Using the facts that

$$\left.\frac{\partial C}{\partial v}\right|_0 = \left.\frac{\partial C}{\partial a}\right|_0 = \mp\frac{4}{\tau}, \tag{B.7}$$

where $\mp$ sign in Equation (B.7) corresponds to the value at $x = \pm\eta_0$, respectively, we consider two modes of perturbations: the symmetric perturbation with respect to the center of the pulse $-\xi_1 = \xi_2 = \xi$ and antisymmetric one $\xi_1 = \xi_2 = \xi$. We apply the Laplace transformation to Equation (B.2) and finally obtain

$$\begin{aligned} -\xi(0) = \Bigg[&-z + \frac{4}{\tau}\Bigg(\frac{1}{2\sqrt{\mu+1}}\left(1 - e^{-2\sqrt{\mu+1}\eta_0}\right) \\ &- \frac{1}{2\sqrt{z+\mu+1}}\left(1 \pm e^{-2\sqrt{z+\mu+1}\eta_0}\right) \\ &+ (1 \pm 1)\alpha\Bigg)\Bigg] \widehat{\xi}(z) \equiv F_\pm(z)\widehat{\xi}(z), \end{aligned} \tag{B.8}$$

where F_+ and F_- correspond to the symmetric and antisymmetric cases, respectively.

C. Traveling Pulse in the Limit of $\varepsilon \longrightarrow 0$

In this appendix, we show the traveling pulse solution of the RD system (1). In the limit $\varepsilon \longrightarrow 0$, the RD system (1) is greatly simplified. Putting $z = x - ct$, the traveling pulse $v(z,t)$ satisfies a time evolution equation

$$\frac{\partial v}{\partial t} = \frac{\partial^2 v}{\partial z^2} + c\frac{\partial v}{\partial z} - (\mu+1)v + H(u-a). \tag{C.1}$$

The stationary traveling pulse solution is obtained under the boundary conditions $v(z) \longrightarrow 0$ in the limit $|z| \longrightarrow \infty$, $v(z_\pm - 0) = v(z_\pm + 0)$, and $dv(z_\pm - 0)/dz = dv(z_\pm + 0)/dz$. The positions of left and right interfaces are denoted by z_- and z_+, respectively, and the final expression of $v(z)$ is

$$v(z) = \begin{cases} C_1 e^{\lambda_+ z} & (z < z_-), \\ C_2 e^{\lambda_- z} + C_3 e^{\lambda_+ z} + \dfrac{1}{\mu + 1} & (z_- \le z \le z_+), \\ C_4 e^{\lambda_- z} & (z_+ < z), \end{cases} \tag{C.2}$$

where $\lambda_\pm = (-c \pm \sqrt{c^2 + 4(\mu + 1)})/2$ and C_i $(i = 1, 2, \cdots, 4)$ are given by

$$\begin{aligned} C_1 &= \frac{\lambda_-}{\lambda_+ - \lambda_-} \frac{1}{\mu + 1} \left(e^{-\lambda_+ z_+} - e^{-\lambda_+ z_-} \right), \\ C_2 &= \frac{-\lambda_+}{\lambda_+ - \lambda_-} \frac{1}{\mu + 1} e^{-\lambda_- z_-}, \\ C_3 &= \frac{\lambda_-}{\lambda_+ - \lambda_-} \frac{1}{\mu + 1} e^{-\lambda_+ z_+}, \\ C_4 &= \frac{\lambda_+}{\lambda_+ - \lambda_-} \frac{1}{\mu + 1} \left(e^{-\lambda_- z_+} - e^{-\lambda_- z_-} \right). \end{aligned} \tag{C.3}$$

The corresponding stationary solution $u(z)$ is given by $u(z) = H(u - a) - v(z)$, and the pulse width l is $l = z_+ - z_-$.

D. Stability Analysis of the Homogeneous Solution of the KT Model

In this appendix, following similar procedure used in ref. [38], we derive the linear growth rate of instability of the spatially homogeneous solution in the KT model (17). In our choice of parameters, there is a spatially homogeneous solution of the RD system (12); $u = v = 0$. We denote as $u_0 = 0$ and $v_0 = 0$. We note that, in the moving coordinate $z = x - ct$, the system has a spatially homogeneous solution (u_0, v_0).

In the moving coordinate $z = x - ct$, the KT model (17) is

$$\varepsilon \frac{\partial u}{\partial t} = \varepsilon^2 \frac{\partial^2 u}{\partial z^2} + \varepsilon c \frac{\partial u}{\partial z} + h(u), \tag{D.1}$$

where $h(u)$ is given by Equation (18) and v in the RD system (12) is expressed by using kernel J in the KT model as

$$v(z) = J * u(z) = \int_{-L}^{L} J(z - y) u(y) dy, \tag{D.2}$$

where $J(z)$ is given by Equation (16). We note that J satisfies

$$\int_{-L}^{L} J(z - y) dy = 0. \tag{D.3}$$

Using this relation, $J * u_0 = 0$, for an arbitrary spatially homogeneous solution u_0. To consider the linear stability of Equation (D.1), we put $u(z, t) = u_0 + \varphi(z, t)$ with a small deviation $\varphi(z, t)$. The corresponding deviation of $J * u(z)$ is given by

$$J * u(z) = \int_{-L}^{L} J(z - y) u(y) dy = J * \varphi(z, t). \tag{D.4}$$

We define the Fourier transformation of $\varphi(z, t)$ as

$$\begin{aligned} \varphi_k(t) &= \mathcal{F}(\varphi(z, t)) = \frac{1}{2L} \int_{-L}^{L} \varphi(z, t) e^{-i(k\pi/L)z} dz, \\ \varphi(z, t) &= \sum_{k=-\infty}^{\infty} \varphi_k(t) e^{i(k\pi/L)z}, \end{aligned} \tag{D.5}$$

where $k = 0, \pm 1, \pm 2, \cdots$. Applying Fourier transformation to Equation (D.1), and putting $\varphi_k(t) = \varphi_k(0) e^{\lambda t}$, we obtain the eigenvalue λ as

$$\begin{aligned} \varepsilon\lambda &= -\left(\frac{\varepsilon k \pi}{L} \right)^2 + i\varepsilon c \left(\frac{k\pi}{L} \right) + \left(\left. \frac{\partial h}{\partial u} \right|_{(u_0, v_0)} \right) + 2LJ_k \left(\left. \frac{\partial h}{\partial v} \right|_{(u_0, v_0)} \right) \\ &= -\left(\frac{\varepsilon k \pi}{L} \right)^2 + i\varepsilon c \left(\frac{k\pi}{L} \right) - a_0 + 2LJ_k, \end{aligned} \tag{D.6}$$

where J_k is

$$\begin{aligned} J_k = \mathcal{F}(J(z)) = \frac{1}{2L} \Bigg[&- \frac{1}{d_1 (\lambda_+ - i(k\pi/L))(\lambda_- - i(k\pi/L))} \\ &+ \frac{1}{d_2 \left(\widehat{\lambda}_+ - i(k\pi/L) \right) \left(\widehat{\lambda}_- - i(k\pi/L) \right)} \Bigg], \end{aligned} \tag{D.7}$$

where $\lambda_\pm$ and $\widehat{\lambda}_\pm$ are given in Section 5. Because a pure imaginary number does not affect the stability of the solution, omitting the second term of Equation (D.6), we finally obtain the growth rate of instability of the spatially homogeneous solution as

$$\lambda = \frac{1}{\varepsilon} \left[-\left(\frac{\varepsilon k \pi}{L} \right)^2 + 2LJ_k - a_0 \right]. \tag{D.8}$$

Data Availability

All data that support the findings of this study are included in the article.

Conflicts of Interest

The author declares that there are no conflicts of interest.

References

[1] P. Zhang, Y. Xue, Y.-C. Zhang, X. Wang, and B.-L. Cen, "A macroscopic traffic flow model considering the velocity difference between adjacent vehicles on uphill and downhill slopes," *Modern Physics Letters B*, vol. 34, no. 21, p. 2050217, 2020.

[2] F. Charru, B. Andreotti, and P. Claudin, "Sand ripples and dunes," *Annual Review of Fluid Mechanics*, vol. 45, pp. 469–493, 2013.

[3] A. M. Morad, E. S. Selima, and A. K. Abu-Nab, "Bubbles interactions in fluidized granular medium for the van der Waals hydrodynamic regime," *The European Physical Journal Plus*, vol. 136, no. 3, article 306, 2021.

[4] E. M. Elsaid, T. Z. A. Wahid, and A. M. Morad, "Exact solutions of plasma flow on a rigid oscillating plate under the effect of an external non-uniform electric field," *Results in Physics*, vol. 19, article 103554, 2020.

[5] T. Z. A. Wahid and A. M. Morad, "On analytical solution of a plasma flow over a moving plate under the effect of an applied magnetic field," *Advances in Mathematical Physics*, vol. 2020, Article ID 1289316, 11 pages, 2020.

[6] A. M. Turing, "The chemical basis of morphogenesis," *Philosophical Transactions of the Royal Society of London. Series B, Biological Sciences*, vol. 237, no. 641, pp. 37–72, 1952.

[7] J. D. Murray, *Mathematical Biology*, Springer-Verlag, Berlin, 3rd edition, 2002.

[8] T. Sushida, S. Kondo, K. Sugihara, and M. Mimura, "A differential equation model of retinal processing for understanding lightness optical illusions," *Japan Journal of Industrial and Applied Mathematics*, vol. 35, no. 1, pp. 117–156, 2018.

[9] L. Chen, K. Painter, C. Surulescu, and A. Zhigun, "Mathematical models for cell migration: a non-local perspective," *Philosophical Transactions of the Royal Society of London. Series B, Biological Sciences*, vol. 375, no. 1807, article 20190379, 2020.

[10] A. Gierer and H. Meinhardt, "A theory of biological pattern formation," *Biological Cybernetics*, vol. 12, no. 1, pp. 30–39, 1972.

[11] S.-I. Amari, "Dynamics of pattern formation in lateral-inhibition type neural fields," *Biological Cybernetics*, vol. 27, no. 2, pp. 77–87, 1977.

[12] A. Hutt, "Effects of nonlocal feedback on traveling fronts in neural fields subject to transmission delay," *Physical Review E*, vol. 70, no. 5, article 052902, 2004.

[13] G. Lv and M. Wang, "Traveling waves of some integral-differential equations arising from neuronal networks with oscillatory kernels," *Journal of Mathematical Analysis and Applications*, vol. 370, no. 1, pp. 82–100, 2010.

[14] L. Solnica-Krezel, Ed., *Pattern Formation in Zebrafish*, Springer-Verlag, Berlin, Heidelberg, 2002.

[15] A. Nakamasu, G. Takahashi, A. Kanbe, and S. Kondo, "Interactions between zebrafish pigment cells responsible for the generation of Turing patterns," *Proceedings of the National Academy of Sciences*, vol. 106, no. 21, pp. 8429–8434, 2009.

[16] S. Kondo, M. Watanabe, and S. Miyazawa, "Studies of Turing pattern formation in zebrafish skin," *Philosophical Transactions of the Royal Society A*, vol. 379, no. 2213, article 20200274, 2021.

[17] A. M. Nakamasu, "Correspondences between parameters in a reaction-diffusion model and connexin functions during zebrafish stripe formation," *Frontiers in Physics*, vol. 9, article 805659, 2022.

[18] S. Kondo, "An updated kernel-based Turing model for studying the mechanisms of biological pattern formation," *Journal of Theoretical Biology*, vol. 414, pp. 120–127, 2017.

[19] S.-I. Ei, H. Ishii, S. Kondo, T. Miura, and Y. Tanaka, "Effective nonlocal kernels on reaction-diffusion networks," *Journal of Theoretical Biology*, vol. 509, article 110496, 2021.

[20] I. Rehberg, S. Rasenat, and V. Steinberg, "Traveling waves and defect-initiated turbulence in electroconvecting nematics," *Physical Review Letters*, vol. 62, no. 7, pp. 756–759, 1989.

[21] J.-H. Huh, "Traveling waves and worms in ac-driven electroconvection under external multiplicative noise," *Physical Review E*, vol. 95, no. 4, article 042704, 2017.

[22] S. Tarama, S. U. Egelhaaf, and H. Löwen, "Traveling band formation in feedback-driven colloids," *Physical Review E*, vol. 100, no. 2, article 022609, 2019.

[23] E. S. Selima, Y. Mao, X. Yao, A. M. Morad, T. Abdelhamid, and B. I. Selim, "Applicable symbolic computations on dynamics of small-amplitude long waves and Davey-Stewartson equations in finite water depth," *Applied Mathematical Modelling*, vol. 57, pp. 376–390, 2018.

[24] A. M. Abourabia and A. M. Morad, "Exact traveling wave solutions of the van der Waals normal form for fluidized granular matter," *Physica A: Statistical Mechanics and its Applications*, vol. 437, pp. 333–350, 2015.

[25] P. W. Bates and F. Chen, "Spectral analysis of traveling waves for nonlocal evolution equations," *SIAM Journal on Mathematical Analysis*, vol. 38, no. 1, pp. 116–126, 2006.

[26] C. Bachmair and E. Schöll, "Nonlocal control of pulse propagation in excitable media," *The European Physical Journal B*, vol. 87, no. 11, article 276, 2014.

[27] J. Siebert, S. Alonso, M. Bär, and E. Schöll, "Dynamics of reaction-diffusion patterns controlled by asymmetric nonlocal coupling as a limiting case of differential advection," *Physical Review E*, vol. 89, no. 5, article 052909, 2014.

[28] B.-S. Han, D.-Y. Kong, Q. Shi, and F. Wang, "Periodic traveling waves and asymptotic spreading of a monostable reaction-diffusion equations with nonlocal effects," *Electronic Journal of Differential Equations*, vol. 2021, no. 22, pp. 1–24, 2021.

[29] S.-I. Ei and H. Ishii, "The motion of weakly interacting localized patterns for reaction-diffusion systems with nonlocal effect," *Discrete and Continuous Dynamical System Series B*, vol. 26, no. 1, pp. 173–190, 2021.

[30] A. L. Hodgkin and A. F. Huxley, "A quantitative description of membrane current and its application to conduction and excitation in nerve," *The Journal of Physiology*, vol. 117, no. 4, pp. 500–544, 1952.

[31] M. Golubitsky, E. Knobloch, and I. Stewart, "Target patterns and spirals in planar reaction-diffusion systems," *Journal of Nonlinear Science*, vol. 10, no. 3, pp. 333–354, 2000.

[32] D. Naoumenko and P. Gong, "Complex dynamics of propagating waves in a two-dimensional neural field," *Frontiers in Computational Neuroscience*, vol. 13, article 50, 2019.

[33] C. Radehaus, R. Dohmen, H. Willebrand, and F.-J. Niedernostheide, "Model for current patterns in physical systems with two charge carriers," *Physical Review A*, vol. 42, no. 12, pp. 7426–7446, 1990.

[34] F.-J. Niedernostheide, M. Ardes, M. Or-Guil, and H.-G. Purwins, "Spatiotemporal behavior of localized current filaments in *p-n-p-n* diodes: numerical calculations and comparison with experimental results," *Physical Review B*, vol. 49, no. 11, pp. 7370–7384, 1994.

[35] U. Middya, M. D. Graham, D. Luss, and M. Sheintuch, "Pattern selection in controlled reaction-diffusion systems," *The Journal of Chemical Physics*, vol. 98, no. 4, pp. 2823–2836, 1993.

[36] K. Krischer and A. Mikhailov, "Bifurcation to traveling spots in reaction-diffusion systems," *Physical Review Letters*, vol. 73, no. 23, pp. 3165–3168, 1994.

[37] S. Kawaguchi and M. Mimura, "Collision of travelling waves in a reaction-diffusion system with global coupling effect," *SIAM Journal on Applied Mathematics*, vol. 59, no. 3, pp. 920–941, 1999.

[38] H. Ninomiya, Y. Tanaka, and H. Yamamoto, "Reaction, diffusion and non-local interaction," *Journal of Mathematical Biology*, vol. 75, no. 5, pp. 1203–1233, 2017.

[39] T. Kappeler and J. Pöschel, *KdV & KAM, A Series of Modern Surveys in Mathematics*, vol. 45, Springer-Verlag, Berlin, Heidelberg, 2003.

[40] T. Ohta, M. Mimura, and R. Kobayashi, "Higher-dimensional localized patterns in excitable media," *Physica D: Nonlinear Phenomena*, vol. 34, no. 1-2, pp. 115–144, 1989.

[41] J. Rinzel and J. B. Keller, "Traveling wave solutions of a nerve conduction equation," *Biophysical Journal*, vol. 13, no. 12, pp. 1313–1337, 1973.

[42] J. Rinzel and D. Terman, "Propagation phenomena in a bistable reaction-diffusion system," *SIAM Journal on Applied Mathematics*, vol. 42, no. 5, pp. 1111–1137, 1982.

[43] E. Yanagida, "Stability of fast travelling pulse solutions of the FitzHugh-Nagumo equations," *Journal of Mathematical Biology*, vol. 22, no. 1, pp. 81–104, 1985.

[44] A. Ito and T. Ohta, "Self-organization in an excitable reaction-diffusion system. III. Motionless localized versus propagating-pulse solutions," *Physical Review A*, vol. 45, no. 12, pp. 8374–8382, 1992.

[45] F.-J. Niedernostheide, B. S. Kerner, and H.-G. Purwins, "Spontaneous appearance of rocking localized current filaments in a nonequilibrium distributive system," *Physical Review B*, vol. 46, no. 12, pp. 7559–7570, 1992.

[46] C. Radehaus, H. Willebrand, R. Dohmen, F.-J. Niedernostheide, G. Bengel, and H.-G. Purwins, "Spatially periodic patterns in a dc gas-discharge system," *Physical Review A*, vol. 45, no. 4, pp. 2546–2557, 1992.

[47] A. Horikawa and J.-H. Huh, "Traveling waves in one-dimensional electroconvection of nematic liquid crystals," *Journal of the Physical Society of Japan*, vol. 88, no. 3, article 034602, 2019.

[48] K. Ikeda, S.-I. Ei, M. Nagayama, M. Okamoto, and A. Tomoeda, "Reduced model of a reaction-diffusion system for the collective motion of camphor boats," *Physical Review E*, vol. 99, no. 6, article 062208, 2019.

[49] H. Schmidt and T. R. Knösche, "Action potential propagation and synchronisation in myelinated axons," *PLoS Computational Biology*, vol. 15, no. 10, article e1007004, 2019.